

# Regularization Methods for Radio Tomographic Imaging

Joey Wilson, Neal Patwari, Fernando Guevara Vasquez  
University of Utah

joey.wilson@utah.edu, npatwari@ece.utah.edu, fguevara@math.utah.edu

*Abstract*—*Radio Tomographic Imaging (RTI)* is an emerging technology that uses received signal strength measurements to image the attenuation of objects within a wireless network area. RTI is by nature an ill-posed inverse problem, therefore, regularization techniques must be utilized to obtain accurate images. This paper discusses some common regularization techniques, including Tikhonov, truncated singular value decomposition, and total variation, and presents the results of applying them to RTI.

## I. INTRODUCTION

*Radio Tomographic Imaging (RTI)* is a method for imaging the attenuation of physical objects within areas surrounded by wireless radios. RTI uses received signal strength (RSS) measurements that traverse the network area to reconstruct an image of where the signals are being attenuated (see Fig. 1). Previous work developed a linear model relating the attenuation field to signal strength measurements, and derived error bounds for resultant images [1], [2]. The formulation for RTI is by nature an ill-posed inverse problem, and regularization must be applied to obtain accurate images. This paper focuses on a few common regularization techniques, and presents the results of applying them to RTI.

RTI has applications in emergencies, rescue operations, and security breaches, since the objects being imaged need not carry an electronic device. RF signals can travel through obstructions such as walls, trees, and smoke, while optical or infrared imaging systems cannot. RF imaging will also work in the dark, where video cameras will fail. Even for applications where video cameras *could* work, privacy concerns may prevent their deployment. An

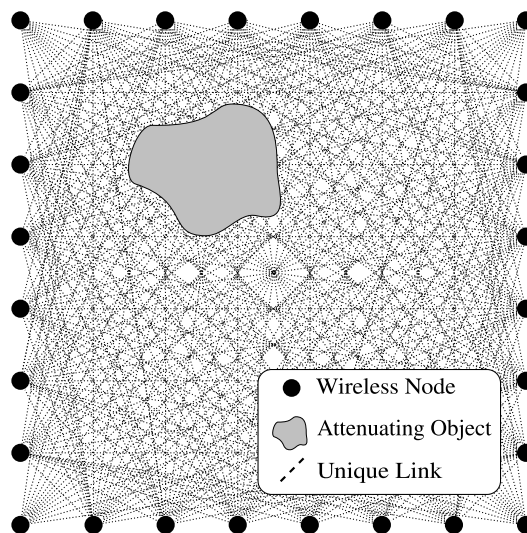


Fig. 1. An illustration of an RTI network. Each node broadcasts to the others, creating many projections that can be used to reconstruct an image of objects inside the network area.

RTI system provides current images of the location of people and their movements, but cannot be used to identify a person.

One main application of RTI is to reduce injury for correctional and law enforcement officers; many are injured each year because they lack the ability to detect and track offenders through building walls [3]. By showing the locations of people within a building during hostage situations, building fires, or other emergencies, RTI can help law enforcement and emergency responders to know where they should focus their attention.

Another application is in automatic monitoring and control in “smart” homes and buildings. Some building control systems detect motion in a room and use it to control lighting, heating, air condition-

ing, and even noise cancellation. RTI systems can further determine how many people are in a room and where they are located, providing more precise control.

Generally RTI has application in security and monitoring systems for indoor and outdoor areas. For example, most existing security systems are trip-wire based or camera-based. Trip-wire systems detect when a person crosses a boundary, but do not track the person when they are within the area. Cameras are ineffective in the dark and have limited view angles. An RTI system could serve both as a trip-wire, alerting when intruders enter into an area, and tracking where are at all times while they are inside, regardless of availability of lighting or obstructions.

The reduction in costs for radio frequency integrated circuits (RFICs) and advances in peer-to-peer data networking have made realistic the use of hundreds or thousands of simple radio devices in a single RTI deployment. Since the relative cost of such devices is low, large RTI networks are possible in applications that may be otherwise impractical.

## II. RELATED WORK

RF-based imaging has been dominated in the commercial realm by ultra-wideband (UWB) based through-the-wall (TTW) imaging devices from companies like Time Domain, Cambridge Consultants, and Camero Tech. These companies have developed products using a phased array of radars that transmit UWB pulses and then measure echoes to estimate a range and bearing. These devices are accurate close to the device, but inherently suffer from accuracy and noise issues at long range due to monostatic radar scattering losses and large bandwidths. Some initial attempts [4] allow 2-4 of these high-complexity devices to collaborate to improve coverage.

To emphasize the small required bandwidth compared to UWB, some relevant research is being called “ultra-narrowband” (UNB) radar [5], [6], [7]. These systems propose using narrowband transmitters and receivers deployed around an area to image the environment within that area. Measurements are phase-synchronous at the multiple nodes around the area. Such techniques have been applied to detect and locate objects buried under ground using

what is effectively a synthetic aperture array of ground-penetrating radars [8]. Experiments have been reported which measure a static environment while moving one transmitter or one receiver [7], and measure a static object on a rotating table in an anechoic chamber in order to simulate an array of transmitters and receivers at many different angles [7], [8], [5]. Because in this paper we use low complexity, non-coherent sensors, we can deploy many sensors and image in real time, enabling the study of tracking moving objects. We present experimental results with many devices in real-world, cluttered environments.

*Multiple-input-multiple-output (MIMO) radar* is another emerging field that takes advantage of multiple transmitters and receivers to locate objects within a spatial area [9]. In this framework, signals are transmitted into the area of interest, objects scatter the signal, and the reflections are measured at each receiver. The scattering objects create a channel matrix which is comparable to the channel matrix in traditional MIMO communication theory. RTI differs from MIMO radar in the same way that it differs from traditional radar. Instead of measuring reflections, RTI uses the shadowing caused by objects as a basis for image reconstruction.

Recent research has also used measurements of signal strength on 802.11 WiFi links to detect and locate a person’s location. Experiments in [10] demonstrate the capability of a detector based on the change in signal strength variance to detect and to identify which of four positions a person is located. Our approach is not based on point-wise detection. Instead, we use tomographic methods to estimate an image of the change in the attenuation as a function of space.

## III. LINEAR FORMULATION

When wireless nodes communicate, the radio signals pass through the physical area of the network. Objects within the area absorb, reflect, diffract, or scatter some of the transmitted power. The goal of an RTI system is to determine an image vector of dimension  $\mathbb{R}^N$  that describes the amount radio power attenuation occurring due to physical objects within  $N$  voxels of a network region. Since voxels locations are known, RTI allows one to know where

attenuation in a network is occurring, and therefore, where objects are located.

If  $K$  is the number of nodes in the RTI network, then the total number of unique two-way links is  $M = \frac{K^2 - K}{2}$ . Any pair of nodes is counted as a link, whether or not communication actually occurs between them. The signal strength  $y_i(t)$  of a particular link  $i$  at time  $t$  is dependent on:

- $P_i$ : Transmitted power in dB.
- $S_i(t)$ : Shadowing loss in dB due to objects that attenuate the signal.
- $F_i(t)$ : Fading loss in dB that occurs from constructive and destructive interference of narrow-band signals in multipath environments.
- $L_i$ : Static losses in dB due to distance, antenna patterns, device inconsistencies, etc.
- $\nu_i(t)$ : Measurement noise and modeling error.

Mathematically, the received signal strength is described as

$$y_i(t) = P_i - L_i - S_i(t) - F_i(t) - \nu_i(t) \quad (1)$$

The shadowing loss  $S_i(t)$  can be approximated as a sum of attenuation that occurs in each voxel. Since the contribution of each voxel to the attenuation of a link is different for each link, a weighting is applied. Mathematically, this is described for a single link as

$$S_i(t) = \sum_{j=1}^N w_{ij} x_j(t). \quad (2)$$

where  $x_j(t)$  is the attenuation occurring in voxel  $j$  at time  $t$ , and  $w_{ij}$  is the weighting of pixel  $j$  for link  $i$ . If a link does not “cross” a particular voxel, that voxel is removed by using a weight of zero. For example, Fig. 2 is an illustration of how a direct LOS link might be weighted in a non-scattering environment. In Section III, an ellipse is used as a simple mechanism to determine LOS weighting.

Imaging only the *changing* attenuation greatly simplifies the problem, since all static losses can be removed over time. The change in RSS  $\Delta y_i$  from time  $t_a$  to  $t_b$  is

$$\begin{aligned} \Delta y_i &\equiv y_i(t_b) - y_i(t_a) \\ &= S_i(t_b) - S_i(t_a) + F_i(t_b) - F_i(t_a) \\ &\quad + \nu_i(t_b) - \nu_i(t_a), \end{aligned} \quad (3)$$

which can be written as

$$\Delta y_i = \sum_{j=1}^N w_{ij} \Delta x_j + n_i, \quad (4)$$

where the noise is the grouping of fading and measurement noise

$$n_i = F_i(t_b) - F_i(t_a) + \nu_i(t_b) - \nu_i(t_a) \quad (5)$$

and

$$\Delta x_j = x_j(t_b) - x_j(t_a) \quad (6)$$

is the difference in attenuation at pixel  $j$  from time  $t_a$  to  $t_b$ .

If all links in the network are considered simultaneously, the system of RSS equations can be described in matrix form as

$$\Delta \mathbf{y} = \mathbf{W} \Delta \mathbf{x} + \mathbf{n} \quad (7)$$

where

$$\begin{aligned} \Delta \mathbf{y} &= [\Delta y_1, \Delta y_2, \dots, \Delta y_M]^T \\ \Delta \mathbf{x} &= [\Delta x_1, \Delta x_2, \dots, \Delta x_N]^T \\ \mathbf{n} &= [n_1, n_2, \dots, n_M]^T \\ [\mathbf{W}]_{i,j} &= w_{ij} \end{aligned} \quad (8)$$

In summary,  $\Delta \mathbf{y}$  is the vector of length  $M$  all link difference RSS measurements,  $\mathbf{n}$  is a noise vector, and  $\Delta \mathbf{x}$  is the attenuation image to be estimated.  $\mathbf{W}$  is the weighting matrix of dimension  $M \times N$ , with each column representing a single voxel, and each row describing the weighting of each voxel for that particular link. Each variable is measured in decibels (dB).

To simplify the notation used throughout the rest of this paper,  $\mathbf{x}$  and  $\mathbf{y}$  are used in place of  $\Delta \mathbf{x}$  and  $\Delta \mathbf{y}$ , respectively.

### Normalized Elliptical Weight Model

If knowledge of an environment were available, one could estimate the weights  $\{w_{ij}\}_j$  for link  $i$  which reflected the spatial extent of multiple paths between transmitter and receiver. Perhaps calibration measurements could aid in estimation of the linear transformation  $\mathbf{W}$ . However, with no site-specific information, we require a statistical model that describes the linear effect of the attenuation field on the path loss for each link.

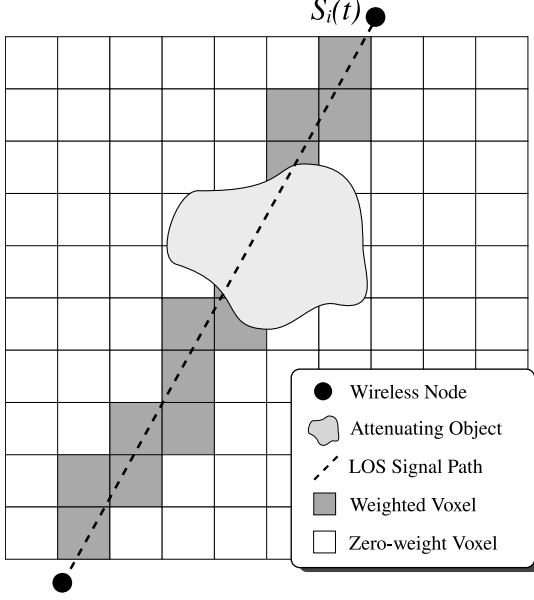


Fig. 2. An illustration of a single link in an RTI network that travels in a direct LOS path. The signal is shadowed by objects as it crosses the area of the network in a particular path. The darkened voxels represent the image areas that have a non-zero weighting for this particular link.

An ellipse with foci at each node location can be used as a method for determining the weighting for each link in the network [1], [2]. If a particular pixel falls inside the ellipse, it is weighted, while all pixels outside the ellipse have a weight of zero. Additionally, the weight for each pixel is normalized by the link length [11]. The weighting is described mathematically as

$$w_{ij} = \frac{1}{\sqrt{d}} \begin{cases} 1 & \text{if } d_{ij}(1) + d_{ij}(2) < d + \lambda \\ 0 & \text{otherwise} \end{cases} \quad (9)$$

where  $d$  is the distance between the two nodes,  $d_{ij}(1)$  and  $d_{ij}(2)$  are the distances from the center of voxel  $j$  to the two node locations for link  $i$ , and  $\lambda$  is a tunable parameter describing the width of the ellipse.

#### IV. REGULARIZATION

Linear models for many physical problems, including RTI, take the form of

$$\mathbf{y} = \mathbf{W}\mathbf{x} + \mathbf{n} \quad (10)$$

where  $\mathbf{y} \in \mathbb{R}^M$  is measured data,  $\mathbf{W} \in \mathbb{R}^{M \times N}$  is a transfer matrix of the model parameters  $\mathbf{x} \in \mathbb{R}^N$ ,

and  $\mathbf{n} \in \mathbb{R}^M$  is a measurement noise vector. When estimating an image from measurement data, it is common to search for a solution that is optimal in the least-squared-error sense.

$$\mathbf{x}_{LS} = \arg \min_{\mathbf{x}} \|\mathbf{W}\mathbf{x} - \mathbf{y}\|_2^2 \quad (11)$$

In other words, the least-squares solution minimizes the noise energy required to fit the measured data to the model. The least-square solution can be obtained by setting the gradient of (11) equal to zero, resulting in

$$\mathbf{x}_{LS} = (\mathbf{W}^T \mathbf{W})^{-1} \mathbf{W}^T \mathbf{y} \quad (12)$$

which is only valid if  $\mathbf{W}$  is full-rank. This is not the case in an RTI system.

RTI is an ill-posed inverse problem, meaning that small amounts of noise in measurement data are amplified to the extent that results are meaningless. This is due to very small singular values in the transfer matrix  $\mathbf{W}$  that cause certain spectral components to grow out of control upon inversion. To see this,  $\mathbf{W}$  is replaced by its singular value decomposition (SVD):

$$\mathbf{W} = \mathbf{U}\mathbf{\Sigma}\mathbf{V}^T \quad (13)$$

where  $\mathbf{U}$  and  $\mathbf{V}$  are unitary matrices, and  $\mathbf{\Sigma}$  is a diagonal matrix of singular values. Plugging (13) into (12), the least squares solution can be written as

$$\mathbf{x}_{LS} = \mathbf{V}\mathbf{\Sigma}^{-1}\mathbf{U}^T \mathbf{y} = \sum_{i=1}^N \frac{1}{\sigma_i} \mathbf{u}_i^T \mathbf{y} \mathbf{v}_i \quad (14)$$

where  $\mathbf{u}_i$  and  $\mathbf{v}_i$  are the  $i$ th columns of  $\mathbf{U}$  and  $\mathbf{V}$ , and  $\sigma_i$  is the  $i$ th diagonal element of  $\mathbf{\Sigma}$ . It is evident that when singular values are small, the corresponding singular basis vectors become very large.

Regularization involves introducing additional information into the mathematical model to handle these small singular values, which makes the inverse problem stable. In some methods, a regularization term  $J(\mathbf{x})$  is added to the objective function of the original problem as

$$f_{reg} = f(\mathbf{x}) + \alpha J(\mathbf{x}), \quad (15)$$

where  $\alpha$  is the weighting parameter. Small values of  $\alpha$  lead to solutions that fit the data, while large values favor the solution that matches prior information.

Some regularization techniques follow from a Bayesian approach, where a certain prior distribution is imposed on the model parameters. Other forms of regularization modify or eliminate small singular values of the transfer matrix. Here, the results of some common regularization methods applied to RTI are examined and compared. An overview of regularization and image reconstruction in general can be found in [12] and [13].

#### A. Tikhonov

In *Tikhonov* regularization, a regularization term is included in the objective function.

$$f(x) = \frac{1}{2} \|\mathbf{W}\mathbf{x} - \mathbf{y}\|^2 + \alpha \|\mathbf{Q}\mathbf{x}\|^2 \quad (16)$$

where  $\mathbf{Q}$  is the *Tikhonov matrix* that enforces a solution with certain desired properties. Taking the derivative of (16) and setting to zero results in the Tikhonov solution:

$$\mathbf{x}_{TIK} = (\mathbf{W}^T \mathbf{W} + \alpha \mathbf{Q}^T \mathbf{Q})^{-1} \mathbf{W}^T \mathbf{y}. \quad (17)$$

Tikhonov regularization provides a simple framework for incorporating desired characteristics into the RTI reconstruction. If smooth images are desired, a difference matrix approximating the derivative of the image can be used in the Tikhonov matrix  $\mathbf{Q}$ . If the prior image is known to have a particular Gaussian covariance structure, the root-inverse covariance matrix  $\mathbf{C}_x^{-1/2}$  can be used.

One major strength of Tikhonov regularization lies in the fact that the solution is simply a linear projection of the measurement data. Since the projection does not depend on instantaneous measurements, it can be pre-calculated, and then applied for various measurements for fast image reconstruction. This is very appealing for realtime RTI systems that require frequent image updates [1], [2].

$$\mathbf{P}_{TIK} = (\mathbf{W}^T \mathbf{W} + \alpha \mathbf{Q}^T \mathbf{Q})^{-1} \mathbf{W}^T \quad (18)$$

$$\mathbf{x}_{TIK} = \mathbf{P}_{TIK} \mathbf{y} \quad (19)$$

#### B. Truncated Singular Value Decomposition (TSVD)

Another common form of regularization called *truncated singular value decomposition (TSVD)* is achieved by removing small singular values from the transfer matrix  $\mathbf{W}$ . In this method, only the

largest  $k$  singular values are kept in the reconstruction shown in (14),

$$\mathbf{x}_{TSVD} = \sum_{i=1}^{k < N} \frac{1}{\sigma_i} \mathbf{u}_i^T \mathbf{y} \mathbf{v}_i = \mathbf{V}_k \Sigma_k^{-1} \mathbf{U}_k^T \mathbf{y} \quad (20)$$

where

$$\mathbf{U}_k = [\mathbf{u}_1, \mathbf{u}_2, \dots, \mathbf{u}_k] \quad (21)$$

$$\mathbf{V}_k = [\mathbf{v}_1, \mathbf{v}_2, \dots, \mathbf{v}_k] \quad (22)$$

$$\Sigma_k^{-1} = \text{diag}(\sigma_1^{-1}, \sigma_2^{-1}, \dots, \sigma_k^{-1}). \quad (23)$$

The TSVD technique is a reduction of the dimensionality of the true solution. It can be thought of as a projection of the solution onto a subspace spanned by the remaining singular vectors. Those singular vectors are dependent on the device itself, or in RTI, the node locations and signal propagation model. Since the projection is based on the device itself, TSVD lacks the ability for incorporation of known or desired image properties into the results.

Like Tikhonov regularization, a transform matrix can be pre-calculated and applied to data for fast image reconstruction in realtime applications.

$$\mathbf{P}_{TSVD} = \mathbf{V}_k \Sigma_k^{-1} \mathbf{U}_k^T \quad (24)$$

$$\mathbf{x}_{TSVD} = \mathbf{P}_{TSVD} \mathbf{y} \quad (25)$$

#### C. Total Variation

*Total Variation (TV)* is a form of non-linear regularization that penalizes changes in the solution. Mathematically, total variation takes the form

$$f(\mathbf{x}) = \frac{1}{2} \|\mathbf{W}\mathbf{x} - \mathbf{y}\|^2 + \alpha TV(\mathbf{x}) \quad (26)$$

where

$$TV(\mathbf{x}) = \sum_i |\nabla \mathbf{x}|_i, \quad (27)$$

and  $|\nabla \mathbf{x}|_i$  is the  $i$ th element of the gradient of  $\mathbf{x}$ . In other words, the integration of gradient magnitude is minimized.

It's not possible to calculate the gradient and Hessian of  $TV(\mathbf{x})$ , which is necessary for most numerical optimization algorithms to converge reliably and quickly. To address this problem, a differentiable function is used as an approximate:

$$TV(\mathbf{x}) \simeq \sum_i \sqrt{\|\nabla \mathbf{x}\|_i^2 + \beta^2}. \quad (28)$$

This approximation is based on

$$|a| = \sqrt{a^2} \simeq \sqrt{a^2 + \beta^2} \quad (29)$$

for small  $\beta$ , which removes the discontinuity at  $a = 0$ . The objective function for total variation becomes

$$f(\mathbf{x}) = \frac{1}{2} \|\mathbf{W}\mathbf{x} - \mathbf{y}\|^2 + \alpha \sum_i \sqrt{\|\nabla \mathbf{x}\|_i^2 + \beta^2}. \quad (30)$$

Using this approximation, the gradient and Hessian information is easily obtained and utilized in a numerical optimization procedure. The parameter  $\beta$  is tunable, and relates to the ‘‘sharpness’’ of the images generated by the TV regularization. Total variation penalizes slow changes in an image, and therefore can lead to images that maintain sharp transitions if parameters are set accordingly.

## V. RESULTS

This section presents images that are reconstructed using the regularization techniques described in Section IV. For each image, the same RTI measurement data  $\mathbf{y}$  and transfer matrix  $\mathbf{W}$  were used, and Table I lists the model and calibration parameters.

Parameter	Value	Description
$N$	28	Number of nodes
$N_c$	2000	Number of calibration frames
$\Delta_p$	.17	Pixel width (m)
$\lambda$	.01	Width of weighting ellipse in (9) (m)

TABLE I  
CALIBRATION AND MODEL PARAMETERS

The experiment is performed in an area with furniture, walls, moving people, and other building structures to provide a rich multipath environment. The wireless network is comprised of twenty eight ‘‘Telosb’’ wireless nodes by Crossbow, and each node operates on the IEEE 802.15.4 specification. A token passing protocol is implemented so that node transmissions do not collide.

The nodes are set up in a square network with a length of 4.2 meters on each side, establishing a network image area of 17.6 square meters (196 square feet). Each side of the square contains eight nodes separated by approximately .6 meters (2 feet), as depicted in Fig. 5. The nodes are placed

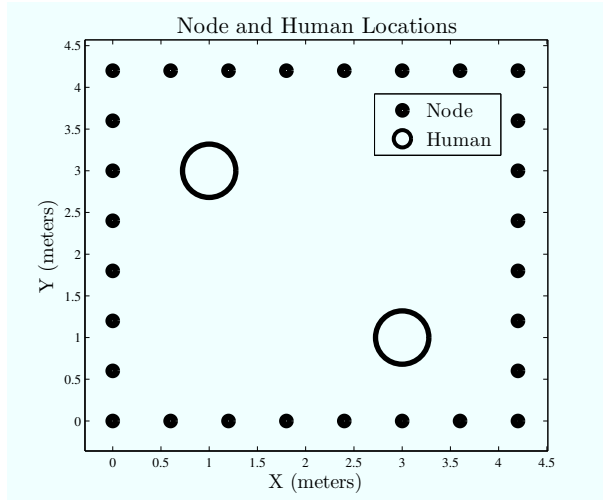


Fig. 5. The RTI geometry and human locations for the images found in Section V. Twenty-eight nodes are placed in a square perimeter, with two humans standing inside the area at coordinates (3,1) and (1,3).

on stands approximately four feet off the ground so that line-of-sight paths travel through humans at torso level.

To image the change in attenuation, RSS measurements of each link are taken at time  $t = t_a$  as described in Section III. During this calibration period, the network area is vacant from moving objects. The signal strength from each link is measured  $N_c$  times and is averaged over the entire calibration period. After calibration, when the RTI network is in use, all instantaneous measurements are taken as the difference from the calibration measurements. This provides the difference measurement vector  $\Delta \mathbf{y}$  in (7), which is required to image motion within the network. In other words, any attenuation that was not part of the calibration at time  $t = t_a$  is imaged.

It should be noted that only one image result is provided for each regularization method. Different regularization parameters will yield different results, but the parameters chosen in this section provided good results in terms of the ability to distinguish the location of changed attenuation. Other parameters were not able to produce significantly better image results in our experiments.

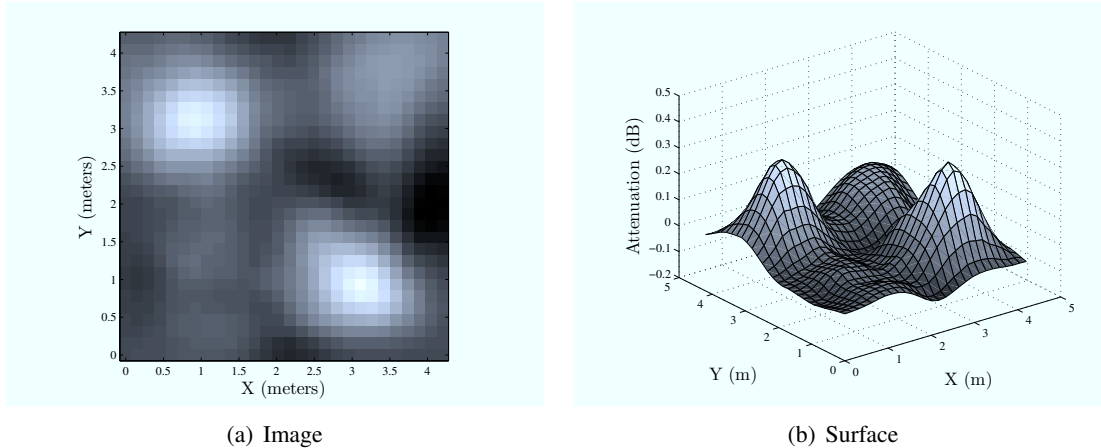


Fig. 3. RTI results using H1 regularization with parameter  $\alpha = 2$  using forward difference matrices.

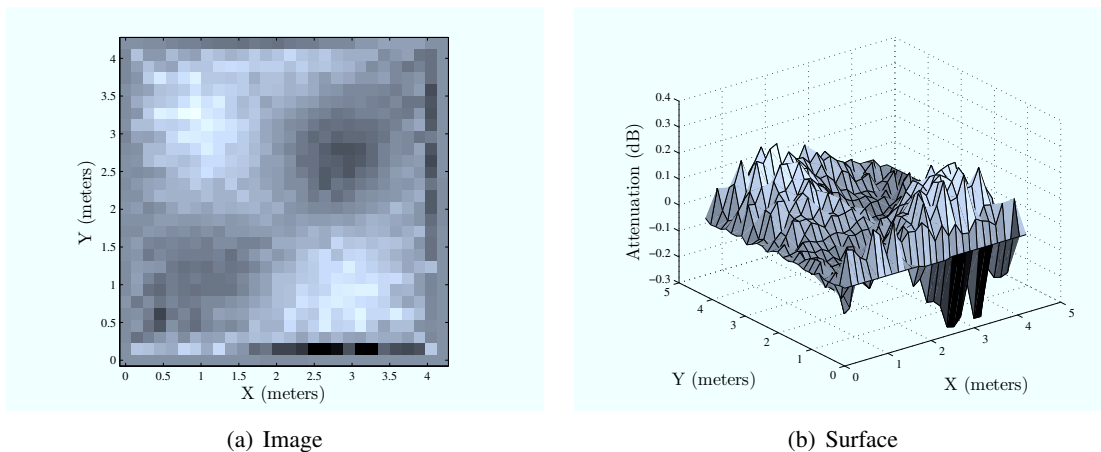


Fig. 4. RTI results using truncated singular value regularization. Here, any singular value below the threshold  $\tau = 5.6$  is truncated.

#### A. Tikhonov

A difference matrix approximating the derivative operator is applied as the Tikhonov matrix  $\mathbf{Q}$ . By minimizing the energy found within the image derivative, noise spikes are suppressed and a smooth image is produced.

Since the image is two dimensional, the regularization should include the derivatives in both the vertical and horizontal directions. The matrix  $\mathbf{D}_X$  is the difference operator for the horizontal direction, and  $\mathbf{D}_Y$  is the difference operator for the vertical direction. The regularized function can be written in this case as

$$f(\mathbf{x}) = \frac{1}{2} \|\mathbf{W}\mathbf{x} - \mathbf{y}\|^2 + \alpha (\|\mathbf{D}_X\mathbf{x}\|^2 + \|\mathbf{D}_Y\mathbf{x}\|^2), \quad (31)$$

which results in the solution

$$\mathbf{x}_{Tik} = (\mathbf{W}^T\mathbf{W} + \alpha(\mathbf{D}_X^T\mathbf{D}_X + \mathbf{D}_Y^T\mathbf{D}_Y))^{-1}\mathbf{W}^T\mathbf{y}. \quad (32)$$

When the derivative is used as the Tikhonov matrix, this is also known as *H1 regularization*.

As seen in Fig. 3, H1 regularization results in very smooth RTI results for  $\alpha = 2$ . The difference operators act as a low-pass filter, smoothing the noise and blurring any sharp changes in attenuation. The smoothness can be increased or decreased by choosing  $\alpha$  appropriately.

#### B. Truncated Singular Value Decomposition (TSVD)

As described in Section IV, TSVD regularization removes spectral components of  $\mathbf{W}$  that correspond

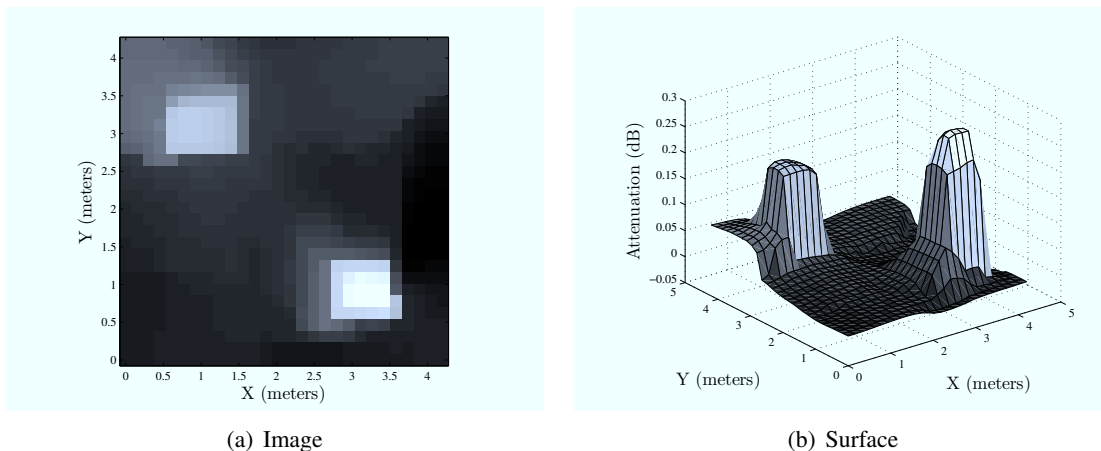


Fig. 6. RTI results using total variation regularization with parameter  $\alpha = .35$  and  $\beta = .08$ .

to low singular values. This means that all information in the spectral components that are removed are entirely lost from the solution.

The limitations of TSVD regularization when applied to RTI are evident in Fig. 4. The image is rough due to the high frequency components that are included in the reconstruction, and yet contrast remains low when the threshold is set to  $\tau = 5.6$ . This makes it difficult for a human or image processing algorithm to determine where objects are located. Other thresholds did not significantly improve the image.

### C. Total Variation

As explained in Section V-A, the gradient of a two-dimensional image is approximated by two difference matrices  $\mathbf{D}_X$  and  $\mathbf{D}_Y$ . This leads to the regularization function for total variation

$$TV(\mathbf{x}) \simeq \sum_i \sqrt{\|\mathbf{D}_Y \mathbf{x}\|_i^2 + \|\mathbf{D}_X \mathbf{x}\|_i^2 + \beta}. \quad (33)$$

The minimum of the total variation least-squares problem is found using a numerical optimization algorithm. In this experiment, the *BFGS* algorithm is used [14].

The total variation results shown in Fig. 6 for  $\alpha = .35$  and  $\beta = .08$  demonstrate the capability of TV regularization in maintaining sharpness of RTI images. The combination of sharp edge definition and low noise make total variation appealing for RTI, but the computational complexity of the numerical optimization is more than Tikhonov or

TSVD regularization. This is due to the fact that the solution must be obtained using a numerical optimization algorithm instead of a simple matrix multiplication, as is the case with Tikhonov and TSVD.

## VI. CONCLUSION

Radio tomographic imaging is an ill-posed inverse problem. Since many different attenuation fields can lead to the same noisy measurement data, no unique solution to the least-squares formulation exists. The problem is made stable by incorporating additional information about the solution into the mathematical framework.

Tikhonov regularization is appealing for RTI systems due to the flexibility to incorporate desired image characteristics into the solution. It follows naturally from a Bayesian approach where the statistical distribution of the image is assumed or known. Since the Tikhonov solution is a linear transformation of the measurement data, it is useful for realtime RTI systems where fast reconstruction of images is needed.

Truncated singular value decomposition is a natural form of regularization that does not require prior information about the solution. This can be viewed as both a strength and a weakness, since it is often helpful to incorporate desired image properties. Our experimental results indicate that TSVD-RTI images are noisier than the other regularization methods, and lack the contrast needed to accurately distinguish the location of moving objects.

Total Variation is useful when the preservation of sharp edges in the image is desired. Experimental results show that TV-RTI images contain a large amount of contrast without much noise, making it easier to distinguish the location of objects. It requires two regularization parameters, however, and is more computationally expensive than the other methods presented in this paper.

The results presented in this paper demonstrate that regularization plays an important role in tracking the location of moving objects with radio tomographic imaging. While this paper presents some common forms of regularization, many other regularization and image reconstruction techniques could be applied to RTI in future work.

#### REFERENCES

- [1] N. Patwari and P. Agrawal, "Effects of correlated shadowing: Connectivity, localization, and RF tomography," in *IEEE/ACM Int'l Conference on Information Processing in Sensor Networks (IPSN'08)*, April 2008.
- [2] J. Wilson and N. Patwari, "Radio tomographic imaging with wireless networks," tech. rep., University of Utah, 2008.
- [3] A. Hunt, C. Tillery, and N. Wild, "Through-the-wall surveillance technologies," *Corrections Today*, vol. 63, July 2001.
- [4] A. R. Hunt, "Image formation through walls using a distributed radar sensor network," in *SPIE Conference on Sensors, and Command, Control, Communications, and Intelligence (C3I) Technologies for Homeland Security and Homeland Defense IV*, vol. 5778, pp. 169–174, May 2005.
- [5] S. L. Coetzee, C. J. Baker, and H. Griffiths, "Narrow band high resolution radar imaging," in *IEEE Conf. on Radar*, pp. 24–27, April 2006.
- [6] *Radar imaging for combatting terrorism*, July/August 2006.
- [7] M. C. Wicks, B. Himed, L. J. E. Bracken, H. Bascom, and J. Clancy, "Ultra narrow band adaptive tomographic radar," in *1st IEEE Intl. Workshop Computational Advances in Multi-Sensor Adaptive Processing*, Dec. 2005.
- [8] M. C. Wicks, "Rf tomography with application to ground penetrating radar," in *41st Asilomar Conference on Signals, Systems and Computers*, pp. 2017–2022, Nov. 2007.
- [9] A. M. Haimovich, R. S. Blum, and L. J. C. Jr., "MIMO radar with widely separated antennas," *IEEE Signal Processing Magazine*, pp. 116–129, January 2008.
- [10] M. Youssef, M. Mah, and A. Agrawala, "Challenges: Device-free passive localization for wireless environments," in *MobiCom*, (Montreal, Quebec, Canada), pp. 222–229, ACM, September 2007.
- [11] P. Agrawal and N. Patwari, "Correlated link shadow fading in multi-hop wireless networks," Tech. Rep. arXiv:0804.2708v2, arXiv.org, Apr. 2008.
- [12] C. R. Vogel, *Computational Methods for Inverse Problems*. SIAM, 2002.
- [13] G. Demoment, "Image reconstruction and restoration: Overview of common estimation structures and problems," *IEEE Transactions on Acoustics Speech and Signal Processing*, vol. 37, December 1989.
- [14] J. Nocedal and S. Wright, *Numerical optimization*. Springer, 1999.